

PROGRESSIVE FAILURE OF EXCAVATED ROCK SLOPES.

by Nicholas Barton\*

SUMMARY

The stability of a rock slope is largely controlled by the presence of discontinuities in the rock. Their presence means that failure is generally of a translational type, and is therefore amenable to simple methods of analysis. The most unstable situation is chosen; one of the joint sets dipping into the slope with a strike direction parallel to the slope face. This situation is amenable to a two dimensional approach. A limit equilibrium method is used to analyse a simple plane failure. Three refinements are then incorporated; the division of the unstable rock mass into slices (representing an additional set of vertically dipping joints), the assumption of zero tensile strength across these slices, and analysis of the effect of excavation on the assumed self weight stress distribution acting on the joints exposed by the excavation. The stability or instability of different parts of the slope is characterised by forces acting parallel to the failure surface. The depth of failure can be calculated without recourse to computing methods. The concept of pre-failure shear displacements and increased weathering of overstressed joints is introduced. This progressive failure mechanism leads to a possible stepped portion of the failure surface. The predicted multi-linear slide scar is characterised by a vertical scarp passing through the crest of the slope, a stepped portion on which the vertical joints open, with sliding on the inclined joints, and shear failure on the inclined joint passing through the toe.

The stepped portion is caused by progressive failure, and residual shear strength parameters are adopted in this region for design purposes. This is considered to be a more realistic solution than a global assumption of residual strength. The method is illustrated by worked examples, in which the progressive failure mode is shown to reduce the failure depth considerably. A further reduction in stability is caused by transient water pressures. The pessimistic assumption of a full tension crack, and steady seepage reducing to zero exit pressure at the toe is used as an illustration.

---

\* Rock Mechanics Engineer, Norwegian Geotechnical Institute, Oslo

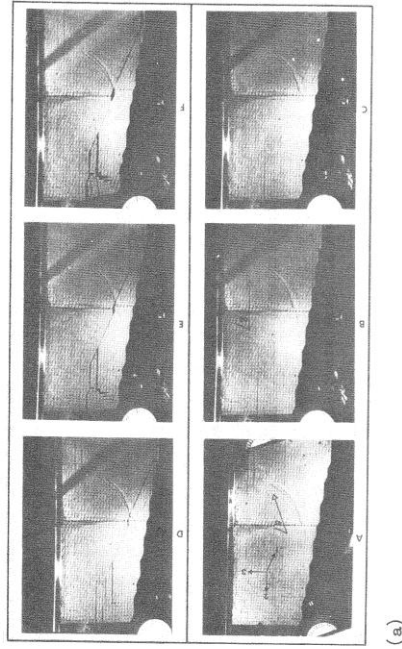
INTRODUCTION

The majority of rock slopes warranting stability investigations will be unstable due to one of two inherent structural features. This could be the chance interaction of the slope with an unfavourably dipping fault surface or with clay filled joints, or alternatively, the eventual overstressing of one or more sets of adversely orientated joints dipping into the slope. The overstressing mechanism may be one of joint water pressure increases caused by poor drainage, or simply due to excavation of the slope to steeper angles or increased cut heights. The failure mechanism may also be initiated by dynamic loading from earthquakes or very large blasts, but this type of loading will not be considered here.

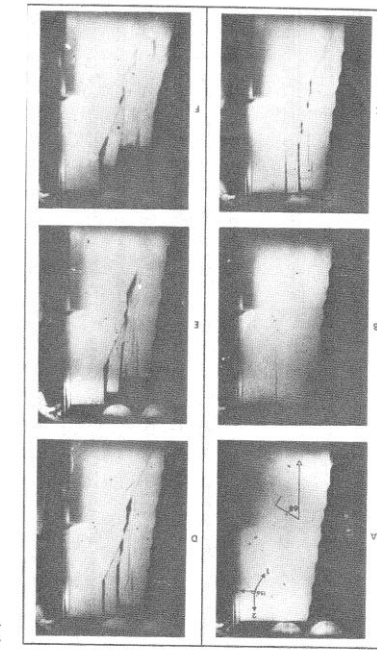
The type of failure to be investigated will be limited to that occurring on adversely dipping joints, associated with at least one further joint set. A two dimensional approach, and consideration of progressive failure lead to the development of a multi-linear failure surface, which has the appearance of a circular slide scar. However, this belies the fact that the mode of failure is purely translational. (Skempton and Hutchinson)<sup>1</sup> There is no rotational component.

The stability of rock slopes has been the subject of several recent papers, in which the three dimensional graphical method of analysis has been utilized (Wittke,<sup>2</sup> Londe,<sup>3</sup> Vigier and Vormerling<sup>4</sup>, and John<sup>5</sup>). There is no doubt that in any open pit excavation there are more potentially adverse rock tetrahedra defined by the intersection of two joint sets, than there are unstable wedges defined by single joint sets. However, the frequency of occurrence is somewhat overshadowed by the fact that potential failures delineated by two shear planes are inherently more stable than those delineated by one shear plane given similar joint dips. At present the graphical methods do not incorporate any stress or limit analysis for determining the position of tension cracks in the unstable tetrahedra, should vertical joints be present. Consequently, the results obtained are dangerously unconservative.

The two dimensional approach which will be adopted here, incorporates sliding on combinations of a single joint set and opening of tension cracks in a secondary joint set. This is the most pessimistic failure mode and consequently the one demanding most attention. Figure 1 shows



(a)



(b)

FIGURE 1. Translational shear and tension crack opening in jointed model slopes that were slowly rotated to induce failure.

the sequential development of this type of translational failure, which was illustrated by models of jointed slopes that were slowly rotated to induce failure.

#### Stresses induced by self weight

It is assumed in the present analysis that all stresses are initiated through self weight loading of a rigid body. This assumption is made in spite of the current fashion for computer produced elastic stress distributions. Mueller and John<sup>6</sup> once suggested that the concept of overburden depth and self weight stresses used in shallow soil slopes was not applicable to steep unsupported rock slopes, due to the severe stress concentrations around the toe of these steep slopes.

These stress concentrations have been indicated in numerous photoelastic and finite element studies of elastic materials. They have also been demonstrated by rock bursts near the base of steep fjord slopes in Norway. However, fjords generally lie at the foot of mountain ridges which are frequently in excess of 5000 feet high. It is well known that such areas are tectonically active. In addition and more importantly, most steep fjord slopes have extremely sparse jointing limited almost entirely to relief or 'sheet' type jointing (Bjerrum and Jorstad<sup>7</sup>).

Recent studies have indicated that elastic stress distributions can be very misleading when applied to normally jointed rock, as encountered in most open pit locations. St. John<sup>8</sup> has suggested that a redistribution of stress can occur in these highly stressed zones due to the discontinuous nature of the jointed rock. This redistribution of stress has been clearly demonstrated by Cundall<sup>9</sup>, from finite difference studies of discontinuous block models of rock slopes.

Large physical models of jointed, excavated rock slopes which were

loaded horizontally (triangular distribution) and by gravity, indicated

that the assumption of a self weight distribution of stress may be the

most valid one, even for steep slopes (Barton<sup>10</sup>).

#### 1. SIMPLE FAILURE ON A SINGLE PLANE

A trivial approach will be followed initially as this helps to clarify the essential elements of the problem. Failure is assumed to occur on the failure surface AB illustrated in Figure 2, with the whole mass

sliding coherently on this plane. The only stresses acting on this failure plane are assumed to be self weight stresses caused by gravity. No joint water pressures are considered for the present.

The shear strength characteristics of the failure plane are assumed (for the purposes of this presentation) to be adequately described by the parameters (c) cohesion intercept, and ( $\phi$ ) angle of friction. A linear shear strength envelope will be assumed, taken as the best piecewise linear approximation to the actual curved envelope.

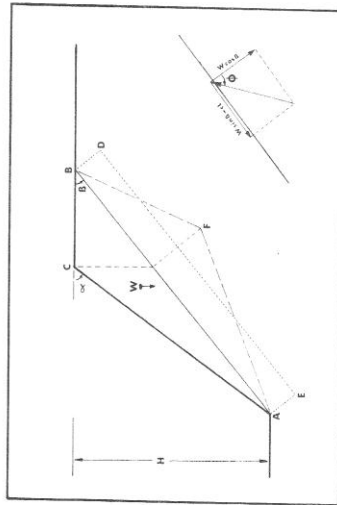


Figure 2. The equilibrium of forces on a planar joint induced by a self-weight stress distribution.

The problem will be further simplified by selecting one pair of (c) and ( $\phi$ ) values as being most relevant to the range of stresses involved. It is frankly admitted that this approach is seldom justified in practice, since an important aspect of slope stability studies is that for any given slope the range of normal stress extends to zero. It is in this region that the shear strength of rock joints is most uncertain, and the traditional (c), ( $\phi$ ) Coulomb assumptions are most in question. However, the errors involved can be significantly reduced by using the relevant curved strength envelope and a computer, and basing the programme on the simple principles which are to be outlined.

From the geometry of Figure 2 the weight of material W above the assumed failure plane AB can be calculated as follows:

$$\begin{aligned} CB &= H(\cot\beta - \cot\alpha) \\ W &= \frac{H^2}{2} (\cot\beta - \cot\alpha) \end{aligned} \quad (1)$$

where:  $H$  = the height of the slope  
 $\bar{x}$  = the average density of the rock mass  
 $\beta^o$  = the inclination of the assumed failure plane  
 $\alpha$  = the inclination of the overall slope

Based on the assumption of self weight stresses, the maximum stress occurs on the failure plane vertically below the crest C. The component of stress perpendicular to AB can be represented by the dashed lines AFB.

It is assumed that this can be approximated to a 'rectangular' distribution of normal stress such as AEDB, where AE is equal to half the height of AFB.

The limiting equilibrium equation describing the normal and shear forces acting on the failure plane is as follows:

$$\tan\phi = \frac{W\sin\beta - cL}{W\cos\beta} \quad (2)$$

where L = the length of failure plane AB =  $H/\sin\beta$

(The third dimension is unity in this two dimensional approach)

Substituting for W and L in equation 2 gives the following relationship:

$$\tan\phi = \tan\beta \left[ 1 - \frac{2c/H}{\cot\beta - \cot\alpha} \sin^2\beta \right] \quad (3)$$

#### Simple Method of slices

Following this trivial approach the wedge of material above the plane AB is now split into parallel-sided slices. Figure 3 illustrates four slices which are chosen such that the dimensions DE and EC are equal, and similarly CF and FB.

Since GF is parallel to AB, triangle CFG is geometrically similar to triangle GBA. Therefore the weights of the four slices are related as follows:

$$W_2 = \frac{1}{2}W_1 \quad W_3 = \frac{1}{2}W_4$$

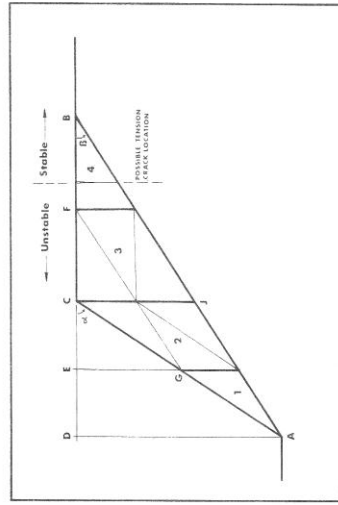


Figure 3. The geometry of four slices dividing an unstable 'wedge'.

It is assumed that the stress distribution beneath each slice can be approximated to a rectangular distribution. The validity of this assumption clearly is increased for larger numbers of slices. The limiting equilibrium equations for the four slices can be obtained by substitution in equation 2. The equations for slices 1 and 2 are as follows:

$$\tan\phi = \tan\beta \left[ 1 - \frac{4c/H}{\cot\beta - \cot\alpha} \sin^2\beta \right] \quad (4)$$

$$\tan\phi = \tan\beta \left[ 1 - \frac{4c/3H}{\cot\beta - \cot\alpha} \sin^2\beta \right] \quad (5)$$

Hence if treated as separate blocks lying on the failure plane, slices 1 and 2 must have different values of cohesion intercept ( $c$ ) or angles of friction ( $\phi$ ), acting across the failure plane for them to both be at limiting equilibrium. Alternatively it can be said that slice 1 is inherently more stable than slice 2 given the same shear strength parameters. The same can be said of slice 4 and slice 3.

#### No-tension concept

This simple idea can be extended by dividing the two triangles AGJ and CJF into a larger number of slices. Given certain conditions, several of the lighter weighted slices could be stable if they could be con-

sidered as independent blocks lying on the failure plane. It will be assumed from now on that the tensile strength of the rock mass in a direction perpendicular to the slice boundaries is zero. This assumption is readily justified if one considers the slice boundaries to represent a parallel set of more or less vertically dipping joints intersecting the rock mass with a strike direction perpendicular to the plane of the figure. The adoption of this "no-tension" concept leads to partial separation of the 'unstable' mass into a possible stable portion lying at the top of the failure plane, and a less stable remainder. The separation between the two parts will be referred to as a tension crack. It is assumed that the tensile nature of the movements across these cracks reduces their shear strength to negligible proportions. Figure 3 illustrates the concept. No tension crack occurs near the bottom of the failure plane since the slice boundaries in this zone will be under compression, if displacements can occur.

It is important to realise that a stability analysis based on the assumption of a coherent wedge sliding on a plane failure surface will generally produce a stability estimate that is under-conservative. That is, the stability of the slope will be overestimated. A simple 'no-tension' assumption is a first step towards improving this estimate, provided that the orientation of one of the joint sets makes the assumption reasonable.

#### Excavation to increased slope heights

The division of the unstable zone into slices will now be extended to include different depths of excavation. Figure 4 illustrates the critical failure planes for four depths of excavation, each with the same slope angle. The steeply dipping planes can be regarded as a persistent set of parallel joints. At each stage of excavation a different joint will be most critically stressed.

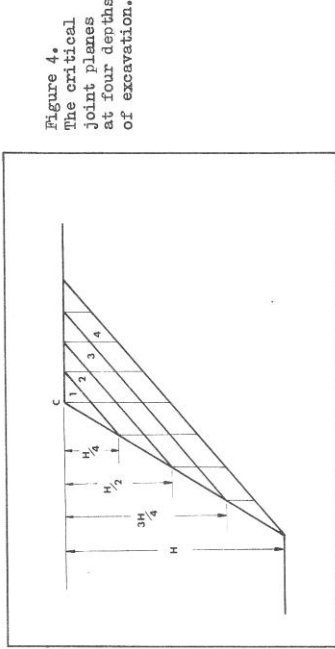


Figure 4.  
The critical  
joint planes  
at four depths  
of excavation.

It is assumed that the presence of joints does not affect the stress distribution compared to an unjointed model. This would probably be valid if no shear displacements occurred on any of the joints. The degree to which the initial stress distribution collapses during progressive failure is of course a subject in itself, and cannot be accounted for in any simple presentation of this type. However, in a global sense the total stress across such failure surfaces remains the same during progressive failure. The discontinuous nature of a rock slope should not be forgotten, when large stress concentrations are imagined. Jointed rock has a considerable potential for redistributing concentrations of stress (Cundall<sup>9</sup>).

The four critical failure planes illustrated in Figure 4 delineate four geometrically similar triangles, each having as their third apex the crest position ( $C$ ). It is a simple matter to modify equation 3 to account for the different limit equilibrium equations describing the slope instability at each depth of excavation. Suppose an unchanged angle of friction was assumed for each failure plane. Then for limiting conditions at each depth of excavation the ratios of cohesion values would need to be as follows.

$$c_4 = \frac{4}{3} \cdot c_3 = 2c_2 = 4c_1$$

This is clearly a hypothetical way of viewing the relative stability at each excavation depth, but it illustrates the obvious point that stability is successively reduced as excavation proceeds. It is parti-

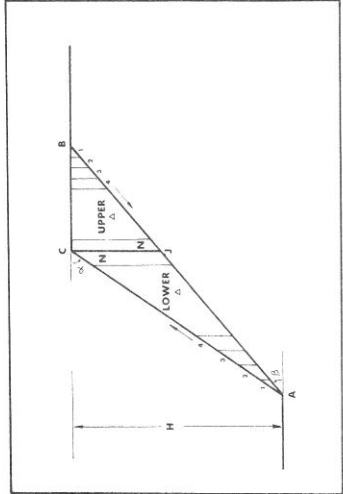


Figure 6. The nomenclature of the slices dividing the upper and lower triangles.

From the geometry of Figure 6 the following limiting equilibrium equations can be obtained:

$$\text{UPPER : } P = \frac{H^2}{2} \cdot (1 - \cot \alpha \tan \beta) \cdot (\cot \beta - \cot \alpha) \cos \beta [\tan \phi - \tan \beta] + \frac{cH(1 - \cot \alpha \tan \beta)}{\sin \beta} \quad (8)$$

$$\text{LOWER : } P = \frac{H^2}{2} \cdot (1 - \cot \alpha \tan \beta) \cdot \cot \alpha \cos \beta [\tan \phi - \tan \beta] + \frac{cH \cot \alpha \tan \beta}{\sin \beta} \quad (9)$$

If both the upper and lower triangles are divided into N slices each, then the individual lengths of the sloping bases beneath each slice are as follows:

$$\text{UPPER : } \frac{1/N \cdot H (1 - \cot \alpha \tan \beta)}{\sin \beta} \quad \Delta \quad \text{LOWER : } \frac{1/N \cdot H (\cot \alpha \tan \beta)}{\sin \beta} \quad \Delta$$

The other variables which are dependent on the slice widths are the weights of individual slices. From the geometrical similarity of Figure 5 it can be verified that the weights of the slices as proportions of the respective upper or lower triangles are:

$$\frac{1}{N^2}, \frac{3}{N^2}, \frac{5}{N^2}, \dots, \frac{2N-1}{N^2}$$

where the slices are taken in order (1 to N) as in Figure 6. Thus, with the nomenclature of Figure 6 the limiting equilibrium equations giving the values of 'unstable excess' for each slice are:

$$\text{UPPER } \Delta: P_{1-N} = \left[ \frac{1,3,5,\dots,2N-1}{N^2} \right] \frac{H^2 \chi}{2} \cdot (1 - \cot \alpha \tan \beta) \cdot (\cot \beta - \cot \alpha) \cos \beta [\tan \phi - \tan \beta] \quad (10)$$

$$\text{LOWER } \Delta: P_{1-N} = \left[ \frac{1,3,5,\dots,2N-1}{N^2} \right] \frac{H^2 \chi}{2} \cdot (1 - \cot \alpha \tan \beta) \cdot \cot \alpha \cos \beta [\tan \phi - \tan \beta] + \frac{1}{N} \cdot \frac{cH(1 - \cot \alpha \tan \beta)}{\sin \beta} \quad (11)$$

where:  $H$  = the height of the slope

$\chi$  = the average density of the rock mass

$\beta$  = the inclination of the assumed failure plane

$\alpha^o$  = the inclination of the overall slope

$c$  = the cohesion intercept exhibited by the failure plane

$\phi$  = the angle of friction exhibited by the failure plane

$N$  = the number of slices dividing each triangle

Solution for  $P$  is simply a matter of substitution. Slices with  $P$  values that are positive are stable individually, and those with negative  $P$  values are unstable. The choice of  $N$  is arbitrary, since once equations 10 and 11 have been reduced to simple expressions by substitution, it takes only a few minutes longer to compute the  $P$  values for twenty slices (total of forty) than for ten slices (total of twenty).

The theoretical existence of a tension crack will be revealed by the  $P$  values obtained for the upper triangle. Taking the slices in order (from 1 to N), if a tension crack exists these  $P$  values will reduce successively from positive values, through zero to increasingly negative values — the greatest of these lying beneath the crest of the slope (the most overstressed position). The position of the tension crack is where the  $P$  value becomes zero. The rock mass above this position will theoretically be stable independently, and failure of the remainder of the slope will be characterised by a slide scar having a vertical rear face (depending on the second joint set) and a planar side surface.

The method will be illustrated by some worked examples before moving on to considerations of progressive failure, which may be induced by excavation.

nent to point out here that if the failure planes (joints) exhibited zero cohesion intercept, then the problem would be dimensionless, and the stability identical for all depths of excavation.

However, since peak shear strength envelopes are curved in reality the problem is far from dimensionless, whether the cohesion intercept (for zero normal stress) is zero or not.

## 2. THE CONCEPT OF AN UNSTABLE EXCESS

It has been established that individual slices will tend to be operating at different 'factors of safety' for equal shear strength parameters. It would therefore be useful if a method were developed, whereby the stability or instability of each slice could be computed separately. Integration of all the slices below the tension-crack would then give a more realistic interpretation to the problem.

An unstable excess concept is proposed, whereby the limit equilibrium equation (equation 2) is generalised to include states of stability other than the limiting case. This method was used for estimating the stability of slices during back analyses of failed slopes (Barton 11).

The stability of any slice is dependent on the magnitude of the forces acting perpendicular and parallel to the failure plane beneath the slice, and on the shear strength exhibited by the failure plane. If the sign of the resultant force  $P$  is positive, this implies that a force of magnitude  $P$ , acting down the plane, is needed to bring that slice to limiting equilibrium. In other words the slice is stable. If on the other hand,  $P$  is negative, this implies an unstable slice which requires a force of magnitude  $P$  acting up the plane to keep the slice from sliding down. The slice has an 'unstable excess' of magnitude  $P$ . It is assumed that any unstable excess will be transmitted to the slice immediately below, but this aspect will be dealt with shortly.

Figure 5 illustrates the equilibrium of forces beneath an individual slice (number  $n$ ) of weight  $W_n$ . The limiting equation is as follows:

$$\tan \phi = \frac{W_n \sin \beta - cL_n + p_n}{W_n \cos \beta} \quad (6)$$

or  $p_n = W_n \cos \beta (\tan \phi - \tan \delta) + cL_n$   
where  $L_n$  = the length of sloping base beneath the slice.

Returning to the geometry of Figure 2 the new limiting equilibrium equation for the whole slope, from equation 6, will be as follows:

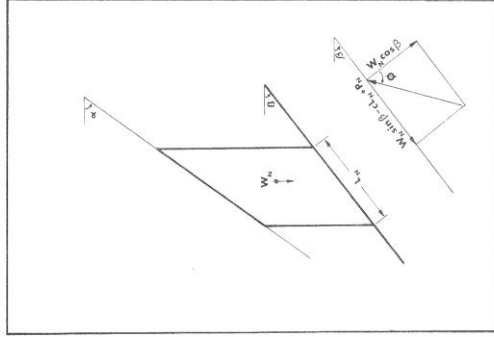


Figure 5. The limiting equilibrium of forces beneath one slice.

$$\frac{P}{2} = \frac{\delta H^2}{2} (\cot \beta - \cot \alpha) + \cos \beta [\tan \phi - \tan \delta] + \frac{c \cdot H}{\sin \beta} \quad (7)$$

It has already been proposed that when splitting a part of the slope into slices, the width of the slices should be made equal to one another. Thus, in the upper triangle  $ABJ$  (see Figure 6) all the slices are of equal width. Likewise, in the lower triangle  $AJ'$ , the widths of the slices are also equal, though not necessarily equal to those of the upper triangle.

It is most convenient to treat the upper and lower triangles separately. It only remains to formulate the two limit equilibrium equations for these two triangles, for the 'unstable excess' values to be obtained for all the individual slices dividing each triangle.

Worked example No. 1.

Firstly, an example will be chosen which illustrates the different results that are obtained when using a slices method, and when analysing the slope as a coherent 'wedge'. Figure 7 illustrates the problem to be considered. Substituting the data in equation 3 (the limiting equilibrium equation for a single coherent 'wedge' lying on a plane failure surface), it is found that failure will occur on one of the steeply dipping joints when the depth of excavation ( $H$ ) exceeds 1000 feet.

However, a method of slices analysis using equations 10 and 11 (assuming that the rock mass exhibits zero tensile strength in a direction perpendicular to the slice boundaries) predicts failure at a depth of excavation appreciably less than 1000 feet, as will be shown.

Substituting the data in equations 10 and 11, the following relations are obtained:

At failure depth

$$\text{Data: } \alpha = 60^\circ, \beta = 50^\circ, \gamma = 100 \text{ lb/ft}^3, \text{ Shear parameters of joints A-B: } c = 1975 \text{ lb/ft}^2, \phi = 45^\circ$$

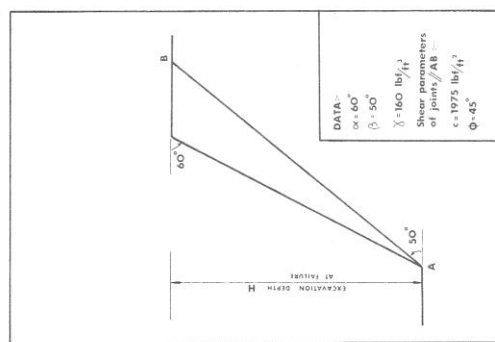


Figure 7. Data for worked example No. 1.

$$\begin{aligned} \text{UPPER } \Delta P_{1-N} &= \frac{1}{1-N} \cdot \frac{2,5 \cdot 2N-1}{N^2} (-8 \cdot 05 \times 10^5) + \frac{1}{N} \cdot (8 \cdot 05 \times 10^5) \frac{\text{lbf}}{\text{ft}} \\ \text{LOWER } \Delta P_{1-N} &= \frac{1}{1-N} \cdot \frac{2,5 \cdot 2N-1}{N^2} (-17 \cdot 75 \times 10^5) + \frac{1}{N} \cdot (17 \cdot 75 \times 10^5) \frac{\text{lbf}}{\text{ft}} \end{aligned}$$

Choosing an  $N = 10$  analysis (total of 20 slices), the  $P$  values of all the slices can be rapidly obtained and are as follows:

(Note: slice nomenclature as in Figure 6.)

**Progressive Failure**

P NUMBER (1 to N)	UPPER $\Delta$		LOWER $\Delta$
	Units:	$10^5 \text{ lbf/ft} \times 10^5$	
P1	[+0.724]	+1.598	
P2	[+0.564]	+1.242	
P3	[+0.402]	+0.887	
P4	[+0.242]	+0.532	
P5	[+0.080]	+0.177	
P6	[-0.080]	-0.177	
P7	[-0.242]	-0.532	
P8	[-0.402]	-0.887	
P9	[-0.564]	-1.242	
P10	[-0.724]	-1.598	

It is important to realise that the striking symmetry of results is strictly a function of the data chosen for this example. The  $P$  values are for slices dividing a 1000 foot slope which is at limiting equilibrium, and their summation ( $P$ ) is equal to zero as would be anticipated.

Since the failure surface is planar the total unstable excess is correctly interpreted as the summation of the individual  $P$  values of each slice. However, as pointed out before, the first few slices of the upper triangle may be stable (positive  $P$  values). These results have been backed in the table above. Thus, in a 'no tension' analysis the overall unstable excess is the summation of all  $P$  values with the exception of the values in brackets.

Hence for  $H = 1000$  ft,  $\Sigma P = -2.013 \times 10^5$  lbf. per foot\*

i.e. the slope has theoretically failed.

(\* per foot refers to the third dimension)

Calculation of failure depth by interpolation

A total of 20 slices ( $N = 10$ ) have been chosen to divide the 1000 ft. slope. From previous arguments it will be apparent that, due to the uniform spacing of the slices, eighteen ( $N = 9$ ) slices of unchanged width will cover 900 feet, sixteen ( $N = 8$ ) slices will cover 800 feet, and so on. (See Figure 4.) Thus, within the results for twenty slices there exists all the information required for calculating the actual depth at which failure occurs. Hence the following table:

No. of slices included (N)	8	9	10
Equivalent depth (feet)	800	900	1000
$\Sigma P$ lbf/foot $\times 10^5$ (feet)	+2.110	+3.09	-2.013

The three results tabulated in the bottom row are sufficient for plotting a graph of depth of excavation versus unstable excess ( $\Sigma P$ ). Where the curve crosses the  $\Sigma P = 0$  line, the equivalent depth of excavation will be that at which limit equilibrium is reached. (See Figure 8.) The shear stress along the failure plane will just have reached the available shear strength.

#### RESULTS

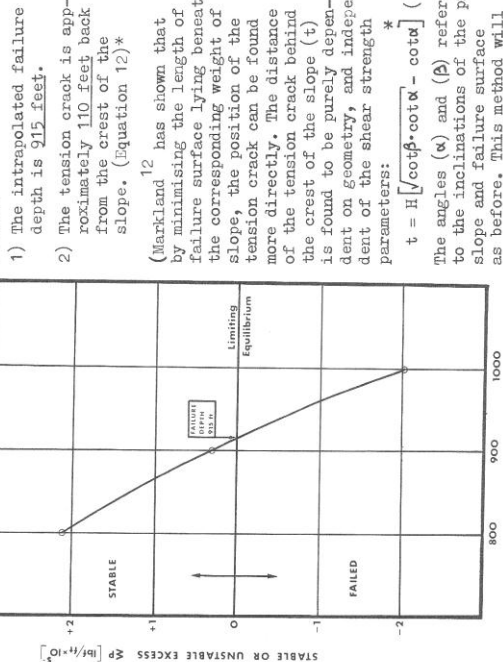


Figure 8. Graph of depth of excavation versus unstable excess

Worked example No. 2 (using metric units)

Problem: At what depth will a pit fail, if excavated at  $60^\circ$  in jointed rock, where one of the joint sets dips into the pit, at an average of  $52\frac{1}{2}^\circ$ ? The shear strength parameters of the joint set are:  $c = 2.5$  tons/m,  $\phi = 45^\circ$ . Density of the rock mass is equal to 2.5 tons/m<sup>3</sup>.

As previously shown, the final result depends upon extrapolation of the results from a particular depth of excavation. The first step is

therefore to make an informed guess of the depth at which failure will occur using equation 7. It is important that this value of H (or a guessed one) is greater than the actual depth of failure, since the result cannot be extrapolated, only interpolated from the P values.

Try H = 100 metres. For an N = 10 analysis, substitution in equations 10 and 11 gives:

$$\begin{aligned} \text{UPPER } P_{1-10} &= \frac{(1,3,5,\dots,19)}{100} (-109.0) + 7.8 \text{ Tens/metre} \\ \text{LOWER } P_{1-10} &= \frac{(1,3,5,\dots,19)}{100} (-329.0) + 23.8 \text{ Tens/metre} \end{aligned}$$

The P values are therefore as follows:

P NUMBER (1 to N)	UPPER Δ	LOWER Δ
Units: Tons/metre		
P1	+6.7	+20.5
P2	+4.5	+13.9
P3	+2.3	+7.3
P4	-0.2	0.8
P5	-2.0	-5.8
P6	-4.2	-12.4
P7	-6.4	-19.0
P8	-8.6	-25.5
P9	-10.7	-32.2
P10	-12.9	-38.7

Slices 1, 2, 3 and 4 of the upper triangle are assumed to be independently stable as before. By selective summation of the P values for different depths of excavation, the second table of results are obtained, from which the failure depth can be extrapolated.

No. of slices included (N)	5	6	7	8
Equivalent depth (metres)	50	60	70	80
$\Sigma P$ tons/metre	+34.7	+48.1	-7.3	-41.4

A plot of the four P values against equivalent depth of excavation indicates that a zero value of P (limiting conditions) is obtained when the depth of excavation is 67.5 metres. Figure 9 illustrates the shape of the slide scar ABCD predicted by this method. AB is the crack which opens up at the surface, BC is the zone which is overstressed (negative P values), and CD is the remaining portion of the failure surface.

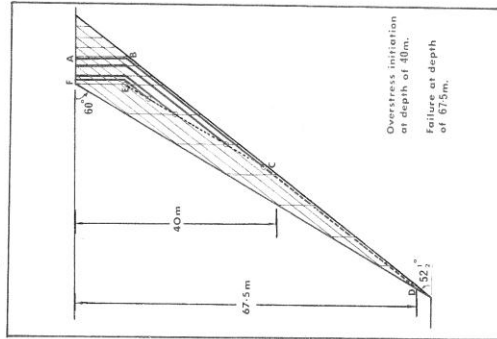
face which fails due to the unstable excess of all the slices lying above it, between C and B.

It will be apparent from the negative  $P$  values (see above table), that parts of several of the unfavourably dipping joints located above BC are also overstressed.

The thick parallel lines shown in Figure 9 represent the lengths of some typical joints which are overstressed. Each of these will have a consequent tension crack opening to the surface. (This theoretical prediction appears to be frequently confirmed in practice.)

The overstressing mechanism is seen to initiate at a depth of 40 metres, and progresses with excavation until, at a depth of 67.5 metres, the total unstable excess becomes greater than the available stable excess. With the given assumptions, failure will be expected on the first joint to intersect the slope at a depth of 67.5 metres or more.

Figure 9. A diagrammatic representation of the overstressed joints predicted by joints predicted by worked example No. 2.



**3. TWO CONCEPTS OF PROGRESSIVE FAILURE**  
Attention will first of all be focussed on the progression of the overstressed zone as excavation proceeds. A second, and most important factor to be considered, is the progressive failure brought about by the unstable shear characteristics of most joint surfaces.

#### A) Progression of overstressed zone

In Figure 9 the lower end of each of the idealized overstressed joints is circled. It is suggested that at these points there exists the

maximum unstable excess for the particular joint in question. One of these joints is illustrated in Figure 10.

The overstressed portion CD, of joint AB, has negative  $P$  values. The area of the shear stress distribution triangle AGB which is in excess of the maximum shear strength level ( $CE = DF$ ) is represented by the shaded area EFG.

Each of the slices between C and D is overstressing the joint surface beneath it, and if shear displacements can occur with the these localized 'failures' then the unstable excess will progressively increase between D and C by simple summation. The slices between C and A will be supporting the full unstable excess of part CD, which is at a maximum at the slice interface above C.

Figure 10. The distribution of shear stress assumed to act on an overstressed joint, before displacements occur.

It is proposed that failure of the rock slope illustrated in Figure 9 could possibly occur on a stepped surface defined by points FEGD, rather than the originally proposed ABCD.

The portion EC is the assumed locus of maximally overstressed points on each critical joint that dips unfavourably into the slope. It is suggested that the rock mass might slide on a stepped surface between B and C, where each step is the secondary joint set (having zero tensile strength). In this way sliding would occur on portions of all the overstressed joints, stepping down progressively from one joint to the

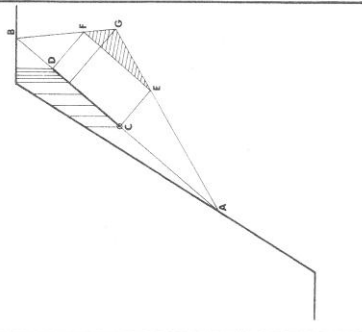


Figure 10. The distribution of shear stress assumed to act on an overstressed joint, before displacements occur.

next immediately beneath. This concept is illustrated diagrammatically in Figure 11.

It should be pointed out that the secondary joint set need not be vertical for this type of failure to be analysed by the proposed methods. The vertical slice boundaries and the vertical steps illustrated so far should just be taken as the most simple method of illustrating secondary joint opening. In reality these artificial planar boundaries between slices could be saw-toothed. (E.g. two orthogonal joint sets dipping at  $45^\circ$  each.) However, it is unlikely that such a system would have zero tensile strength in a horizontal direction, and in any case in practice at least one near-vertical joint set can be expected, more commonly two.

The stability of the stepped and direct failure modes illustrated in Figure 11 were checked, and compared with the original failure surface ABCD. The parameters of worked example No. 2 were used, with unchanged shear strength values:

- (a) Stepped shear surface.  $P = +42.9$  tons/metre (stable)

Note: CE is parallel to the  $60^\circ$  slope DF. However, the actual sliding surface is parallel to the joint dip of  $52\frac{1}{2}^\circ$ . The consequent reduced length of shear surface is accounted for in the above.

- (b) Direct shear surface.  $P = +4.6$  tons/metre (just stable)

Note: It was assumed that both shear and normal components of stress would be transmitted across the vertical slice boundary above

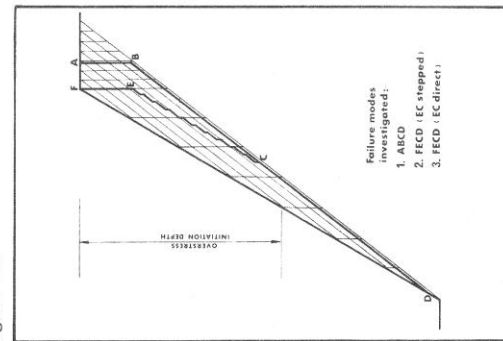


Figure 11. The multi-linear failure surfaces investigated.

point C. The unstable excess for the upper surface ( $60^\circ$  dip) was resolved into the dip direction of the lower surface ( $52\frac{1}{2}^\circ$ ), by the correcting factor:  $\cos(60^\circ - 52\frac{1}{2}^\circ)$ . This method has been used previously (Barton 11) for integrating the unstable excess of slices lying on differently inclined failure surfaces, when back-analysing failed slopes.

The latter mode of failure, although apparently predicting greater instability, is questionable because it will not be feasible unless the rock is very highly jointed. The location of the failure surface might then be independent of the structural discontinuities.

However, it is generally agreed that a 'circular stability analysis' can be usefully applied to rock slopes when the dimensions of the slope are very large compared to the joint spacing. The problem then approaches the soil mechanics end of the spectrum, and a rotational failure mode which is not structurally controlled can be anticipated, rather than failure mode No. 3 in Figure 11.

However, the more usual rock mechanics problem is one of relatively wide joint spacing. The potential failure surface is then almost totally controlled by structural discontinuities. Translational shearing then becomes the dominant mode of failure.

The progression of the overstressed zone as excavation (or erosion) proceeds has been illustrated as a possible mechanism for inducing a stepped multi-linear failure surface. (Mode No. 2 Figure 11). However, this mode of failure has been shown to be the most stable when using unchanged peak shear strength parameters.

Consequently a second mechanism of progressive failure has to be invoked to justify consideration of the stepped failure mode. This concerns the effects of displacement and weathering on the shear strength of joints in-situ.

#### B) Unstable joint characteristics

The shear strength parameters of rock joints have been idealized to those shown in Figure 12. The curved peak strength envelope is approximated to a straight line displaying (c) and (q) parameters appropriate to a particular range of normal stress. Since this range is limited at low stress it may be necessary to interpret the curve in a piece-wise linear fashion.

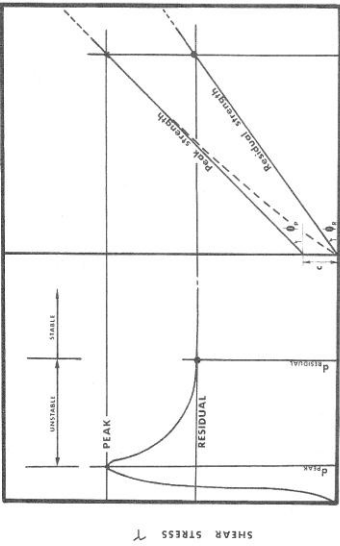


Figure 12. The simplified direct shear characteristics of an interlocking joint surface.

It will be noted that peak shear strength is reached after relatively small shear displacements. In addition the strength can drop significantly for displacements only a little greater than the peak displacements.

However, before peak or residual strength characteristics can be meaningfully applied to parts of an unstable slope, certain questions need to be considered.

1. Can relative shear displacements occur within the overstressed zone of the rock slope before final failure is approached?
2. If so, will the 'slices' at the lower (down dip) ends of the overstressed joints be those most highly overstressing the joints concerned in shear?
3. Will the fact that parts of the joints became overstressed at a relatively early stage of excavation, mean that their shear strength will have reduced by the time the failure depth is approached?
4. If displacements can occur within the rock slope, will these be large enough for a significant reduction from peak shear strength towards residual strength?

It is believed that the answer to all four questions is 'yes'. However, it is realised that positive answers depend upon No. 1 being true. Certain observations can be cited in support.

- (a) Mueller<sup>13</sup> has referred to slope bulging in the lower half of rock slopes of from 7 to 8% of the slope height. This exceptional figure was presumably for a slope in an advanced state of collapse.
- (b) Tension cracks are regularly found at and behind the crest of slopes. Exceptionally these can be ten or more feet wide. A graben is often in evidence; the unstable portion below the crack having fallen vertically several feet. Ross Brown and Barton<sup>14</sup> recorded vertical and horizontal displacements of 5 and 2 metres respectively, at the crest of a 100 metre high slope that was in the process of failing. Kennedy and Niermeyer<sup>15</sup> recorded vertical and horizontal displacements of up to 2.5 and 5 metres respectively. This was measured on a bench roughly in the middle of the enormous Chuquicamata slide, approximately two weeks before catastrophic failure occurred.
- (c) The excavated slope models reported by Barton<sup>10</sup> indicated significant down dip displacements on unfavourably dipping joints. These tended to be greatest where the overburden depth was greatest.
- Down dip shearing displacements imply closure of joints in a direction at right angles to the joints, if one assumes zero shear stresses at the free face of the excavation. Figure 10 illustrates the distribution of shear stress on a typical joint that is obtained when analysing the situation with self weight stress assumptions. The shear stress on AB builds up from zero at the free face (A) to a maximum beneath the crest of the slope. If there are joint sets intersecting AB, then closure across these can be expected, due to the incremental increase in shear stress when proceeding from A towards C. (The effect of shear stress on the pre-peak displacements occurring across tension joints and the closure of joints under normal stresses has been discussed by Barton.<sup>10</sup>) It has also been shown that small shear displacements induced across an interlocking joint surface can cause considerable increases in joint

volume, depending upon the joint roughness. In an area of significant rainfall, this increase in effective permeability would surely accelerate the process of joint weathering. Over a period of time the shear strength of joint walls might be considerably reduced. In view of the fact that open pit mining operations are frequently in excess of 30 years duration, it is possible that rock slopes could be excavated in which overstressing of the peak strength of the joints initiated ten or more years before the final depth of the pit was reached.

It appears a practical possibility that residual strength could be approached on the critical stepped failure surfaces introduced earlier. From a design point of view such an assumption would surely be a more realistic 'worst case' than assigning a universal residual strength to the whole slope. Even in extreme cases slope failure is hardly a dimensionless problem.

An opposite point of view and one which is considered somewhat under-conservative, is that of Jennings and Robertson<sup>16</sup>, and Jennings<sup>17</sup>, who developed an involved 'mathematical' treatment to account for the non-continuous nature of joints. They considered a stepped failure surface involving sliding down one joint set, opening on a second joint set and shear and tensile failure of the intact rock between the two. Some of the parameters involved are almost impossible to estimate in the field.

For this reason the approach adopted by Terzaghi<sup>18</sup> is considered more useful. He suggested that the rock bridges between joints would in all probability be eliminated by splitting, when the shearing stresses rose significantly due to erosion or excavation of the slope concerned. It is anyway safer to design slopes on ( $c$ ) and ( $\phi$ ) parameters no larger than those obtained from shear tests on continuous joints. The contribution of any failure through intact material is best ignored for design purposes.

#### 4. ANALYSIS OF MULTI-LINEAR FAILURE SURFACE

Figure 13 represents a section through an idealized jointed rock slope. It is assumed that the strike of the joints in relation to the slope face, allows the problem to be analysed in two dimensions. As already indicated this is the worst case from the point of view of stability.

In the absence of computing methods, or design charts such as those developed by Hoek<sup>19</sup>, the failure depth ( $H$ ) for a fully drained block 'TGD' will be found by utilizing equations 10 and 11.

The position of the corresponding tension crack 'TC' can be most easily found by using equation 12 (Marland<sup>12</sup>).

$$\text{thus: } AT = H \left[ \sqrt{\cot \alpha \cdot \cot \beta} - \cot \alpha \right]$$

The proposed failure surface 'AGF' conveniently divides the unstable part of the slope into two portions:

1. The block 'AGF', lying on the stepped surface 'EG'. The mean dip of 'EG' is parallel to the slope face 'AF'. Since residual strength is envisaged for the stepped surface (for design purposes), it will be termed the 'residual block'.

2. The 'toe triangle' 'FGD'. Peak strength parameters are suggested for the planar surface 'GD'.

#### A) Estimation of failure depth for a drained slope

(a) The dimensions of the residual block 'AGF' are obtained from the geometry of Figure 13.

$$AB = H \left( \cot \beta - \cot \alpha \right) \quad \text{and} \quad TC = TB \cdot \frac{AJ}{AB}$$

$$\therefore AB = H \left( 1 - \cot \alpha \cdot \tan \beta \right) \left( \cot \beta - \sqrt{\cot \alpha \cdot \cot \beta} \right) \quad (13)$$

$$NA = H \cot \alpha \quad \text{and} \quad MA = NA \cdot \frac{EJ}{AJ} = NA \cdot \frac{AJ}{AB}$$

$$\therefore MA = H \frac{\cot \alpha / \left( \cot \alpha \cdot \cot \beta - \cot \alpha \right)}{\left( \cot \beta - \cot \alpha \right)} \quad (14)$$

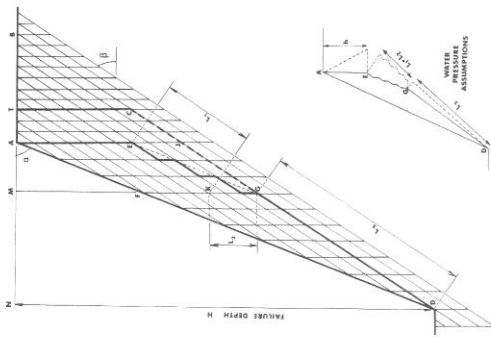


Figure 13. The detailed geometry of the multi-linear failure surface.

Since  $A_E = FG$ :

1. the area of the 'residual block'  $AEGD = AD \cdot MA$
2. the length of shear surface beneath it =  $L_1$   
where  $L_1 = MA \cdot \sec\beta$

The unstable excess ( $P_1$ ) of this block is given by equation 6, thus:

$$P_1 = W_1 \cos\beta [\tan\phi_r - \tan\beta] \quad (15)$$

(Note residual parameters:  $\phi = \phi_r$ ,  $c = 0$ .)

(b) The dimensions of the toe triangle FGD are obtained in a similar manner:

$$\begin{aligned} FG &= AE = TC \quad (\text{equation 13}) \\ NM &= NA \cdot \frac{TB}{AB} = \frac{H \cdot \cot\alpha (\cot\beta - \sqrt{\cot\alpha \cdot \cot\beta})}{(\cot\beta - \cot\alpha)} \quad (16) \end{aligned}$$

1. the area of the 'toe triangle' FGD =  $\frac{1}{2} \cdot FG \cdot NM$
2. the length of shear surface beneath it =  $L_2$   
where  $L_2 = NM \cdot \sec\beta$

If peak strength parameters are assumed for the surface DG, then the stable excess ( $P_2$ ) is given by:

$$P_2 = W_2 \cos\beta [\tan\phi_p - \tan\beta] + cL_2 \quad (17)$$

For complete failure on the multi linear surface AEGD, the unstable excess of the residual block must just exceed the stable excess for the toe triangle. At limiting conditions:

$$P_1 + P_2 = 0$$

The failure depth is obtained by evaluating equations 13 to 17 in general terms, with H the unknown. Several values of H can then be substituted (all less than for block FGD). A graph of stable or unstable excess plotted against depth H will give an intercept  $\Sigma P = 0$  at the required failure depth. (See Figure 8 for example.)

#### B) Estimation of failure depth for a transient water pressure assumption

It is believed that the above assumption of residual shear strength for the stepped portion of the failure surface represents a realistic 'worst case' for design purposes. However, there are many situations which also require pessimistic assumptions for possible water pressure

distributions. Of the five slope failures investigated in the Rio Tinto area of southern Spain (Ross Brown and Barton<sup>14</sup>), three were almost certainly caused by the surface run off entering tension cracks through fractured drainage routes. The possibility of tension cracks becoming filled with water must therefore be considered in areas where flash floods and consequent transient water pressures can be anticipated.

The water pressure distribution assumed as one possible 'worst case' is shown in the inset to Figure 13. The full tension crack generates a hydrostatic pressure at its base of:

$$U_w = hX_w$$

where  $h$  = the depth of crack is given by equation 13, and  $X_w$  is the density of water. It is assumed that this pressure reduces linearly in proportion to the length of drainage path, such that at D the exit seepage pressure is zero. It may be optimistic to expect constant permeability down the length of EGD. However, there are in reality an infinite variety of possible assumptions. A tension crack only partially filled with water, and a reduced permeability along EGD is an alternative which could generate equal instability to the one assumed.

Some attention may need to be paid to the equilibrium of the slide mass, since a severe assumption of water pressure can lead to zero effective pressures across the potential shear surfaces. Whether this could be expected at failure is not known.

From the geometry of Figure 13 :

- 1) Depth of tension crack  $h = AE = TC$  (equation 13)
- 2) Length of inclined surface  $L_1 = MA \cdot \sec\beta$  (equation 14)
- 3) Total length of vertical steps between E and G =  $L_2$   
where  $L_2 = \frac{AD \cdot \cot\alpha}{AB}$
- 4) Length of inclined surface between G and D =  $L_3$   
where  $L_3 = NM \cdot \sec\beta$  (equation 16)

The mean water pressures assumed to act on the four surfaces above are as follows:

- 1)  $AE$  (length  $h$ )  $U_w = \frac{1}{2}hX_w$  (19)  
This has force components perpendicular and parallel to the dip

direction ( $\beta$ ) of:

$$\begin{aligned} & \text{(a) } \frac{1}{2}h\delta_w^2 \sin\beta \\ & \text{(b) } \frac{1}{2}h\delta_w^2 \cos\beta \\ 2) \quad & \text{EG (length } L_1 + L_2) \\ & \text{Since the pressure at G is } \left[ \frac{L_3}{L_1 + L_2 + L_3} \right] h\delta_w \end{aligned}$$

the mean water pressure between E and G is:

$$\left[ \frac{L_1 + L_2 + 2L_3}{L_1 + L_2 + L_3} \right] \frac{h\delta_w}{2} \quad (20)$$

(a) This is distributed on the vertical steps of length  $L_2$  with components  $\sin\beta$  and  $\cos\beta$  as before.

(b) It is also distributed on the inclined surfaces of length  $L_1$  ( $L_1$  is perpendicular component only.)

$$3) \quad \text{GD (length } L_3) \quad \text{The mean water pressure is } \left[ \frac{L_3}{L_1 + L_2 + L_3} \right] \frac{h\delta_w}{2} \quad (21)$$

The failure depth for these transient water pressure assumptions is obtained by calculating the unstable excess ( $P_1$ ) of the residual block ABGF, and the stable excess ( $P_3$ ) of the toe triangle EGD. Once again, at failure:

$$P_1 + P_3 = 0$$

The limiting equilibrium equation for the residual block can be derived from equation 6. The tangent of the friction angle is equated to the ratio of forces acting parallel to the dip ( $\beta$ ), and those acting perpendicular to it, thus:

$$\frac{\tan\phi}{W_1 \sin\beta + \frac{1}{2}h\delta_w^2 \cos\beta + \left[ \frac{L_1 + L_2 + 2L_3}{L_1 + L_2 + L_3} \right] \frac{h\delta_w}{2} \cdot L_2 \cos\beta - cL_1 + P_1} = \frac{W_1 \cos\beta - \frac{1}{2}h\delta_w^2 \sin\beta - \left[ \frac{L_1 + L_2 + 2L_3}{L_1 + L_2 + L_3} \right] \frac{h\delta_w}{2}}{L_2 \sin\beta - \left[ \frac{L_1 + L_2 + 2L_3}{L_1 + L_2 + L_3} \right] \frac{h\delta_w}{2} \cdot L_1 \cos\beta - \left[ \frac{L_1 + L_2 + 2L_3}{L_1 + L_2 + L_3} \right] \frac{h\delta_w}{2} \cdot L_1 \sin\beta} \quad (22)$$

Hence  $P_1$ . Note: For residual parameters,  $\phi = \phi_2$ ,  $c = 0$ .

The limiting equilibrium equation for the toe triangle is:

$$\tan\phi_P = \frac{W \sin\beta - cL_2 + P_3}{W_3 \cos\beta - \left[ \frac{L_3}{L_1 + L_2 + L_3} \right] \frac{h\delta_w}{2}} \quad (23)$$

#### WORKED EXAMPLE

The parameters of worked example No. 1 will be used to illustrate the effects of the given failure mode on stability. (See Figure 7).

$$\begin{aligned} \alpha &= 60^\circ & \phi_p &= 45^\circ \\ \beta &= 50^\circ & c &= 1975 \text{ lbf/ft. per ft.} \end{aligned}$$

The residual shear strength parameters will be assumed as follows:

$$\phi_r = 30^\circ, \quad c = 0 \quad (20)$$

Substitution of the peak shear strength parameters resulted in the following estimates of failure depth. (See Figure 13 for lettering.)

1. Coherent wedge ABD sliding on plane DB with no tension crack.  
 $H = 1000$  feet. Fully drained. Equation 7.
2. Block ABCD. Method of slices and tension crack separation.  
 $H = 915$  feet. Fully drained. Equations 10 and 11.

Equations 13 to 17 were used to calculate the failure depth for the assumption of a multi-linear failure surface, with residual strength on the stepped surface between E and G. With the given geometry, and fully drained conditions:

$$\begin{aligned} 3) \quad AE &= 0.171 \text{ H feet} & NM &= 0.214 \text{ H feet} \\ MA &= 0.264 \text{ H feet} & L_3 &= 0.489 \text{ H feet} \\ P_1 &= (-)2.84 H^2 \text{ (lbf/foot)} & P_3 &= 965 \text{ H} - 0.524 H^2 \text{ (lbf/foot)} \\ \therefore \Sigma P &= P_1 + P_3 = 965 \text{ H} - 3.364 H^2 \text{ lbf/foot} \end{aligned}$$

A graph of  $\Sigma P$  versus  $H$  gives the failure depth as 290 feet

Equations 18 to 23 were used to calculate the failure depth for the transient water pressure assumptions. Once again residual parameters were taken to describe the remaining shear strength on the stepped part of the failure surface.

$$\begin{aligned} 4) \quad L_1 &= 0.264 \text{ H feet} & P_1 &= (-)6.92H^2 \text{ lbf/foot} \\ L_2 &= 0.143 \text{ H feet} & P_3 &= 965 \text{ H} - 1.747 H^2 \text{ lbf/foot} \\ \therefore \Sigma P &= P_1 + P_3 = 965 \text{ H} - 8.587 H^2 \text{ lbf/foot} \end{aligned}$$

A graph of  $\Sigma P$  versus  $H$  gives the failure depth as 115 feet

It should be noted that the above assumption of a full tension crack

(for a given geometry and density) generated such high water pressures that the effective normal stress on the inclined shear surfaces below the residual block just became negative. In other words the shear strength assumptions for this surface became meaningless. However, the effective normal stresses beneath the toe triangle remained positive with the given seepage assumption.

It may be argued that this state of affairs is preferable to one in which assumptions of poor drainage cause the toe triangle to 'float'.

However, this only serves to highlight the uncertainties of what form stress distributions can take at failure. An effective normal stress reducing to zero locally is certainly an ideal failure mechanism. Is it right to reject it purely from a subjective assessment of what seems possible?

#### CONCLUSIONS

The following observations should be made as qualifications to the multi-linear failure mode:

1. The ratio of the depth of tension crack ( $T_c$ ) to the depth of the shear surface beneath the crest ( $A_J$ ) was found by a limit analysis. This was performed with the assumption of drained conditions, and for a particular geometry.
2. The ratio determined what proportion of the total shear surface ( $L_1 + L_3$ ) was stepped ( $L_1$ ). This proportion was assumed constant for a given geometry for all states of stress. In other words, for all conditions which produced failure, a geometrically similar shear surface was assumed.
3. The concept of a multi-linear failure mode was based on the effect of excavation on the overstressing of joints. The weakening mechanisms of time and displacement were introduced to predict a failure surface with a stepped portion of reduced strength. The adoption of residual strength for this part of the failure surface led to considerably reduced failure depths. (i.e. 915 feet down to 290 feet). Paradoxically, if the slope was designed to the reduced height in the first instance, then in all probability the stepped/residual mode would not initiate. Consequently, the proposed methods are conservative, and serve to emphasize

the severity of a global residual strength assumption.

3. The multi-linear residual failure mode has been demonstrated as being readily amenable to manual methods of analysis, when using simple assumptions of geometry and shear strength. Having established the philosophy of the method it is advantageous to computer programme the analysis so that more realistic in-situ data can be incorporated, should this be available. This might include a non-linear peak shear strength envelope based on a statistical analysis of the joint roughness (Barton<sup>20</sup>), and more detailed information concerning joint structures and water pressures.

#### REFERENCES

1. Skempton, A.W. and Hutchinson, J.N. Stability of natural slopes and embankment foundations. State of the art report. VIIIth Int. Conf. Soil Mech. Found. Eng. Mexico 1969, pp. 291-341.
2. Witke, W. A numerical method of calculating the stability of slopes in rocks with systems of plane joints. English translat. Imp. Coll. Rock Mech. Res. Rept. No. 4 Sept. 1970. (From original in German: Rock Mech. and Eng. Geol. Suppl. I. 1964.)
3. Londe, P. and Vigier, G. and Vormeritzer, R. Stability of rock slopes, a three dimensional study. J. Soil Mech. Found. Div. Proc. A.S.C.E. S.M.1., Jan. 1969 pp. 255-262.
4. Londe, P. and Vigier, G. and Vormeritzer, R. Stability of rock slopes - graphical methods. J. Soil Mech. Found. Div. Proc. A.S.C.E. S.M.4. July 1970, pp. 1411-1424.
5. John, K.W. Graphical stability analyses of slopes in jointed rock. J. soil Mech. Found. Div. Proc. A.S.C.E. S.M.2. March 1968 pp. 491-526.
6. Mueller, L. and John, K.W. Recent development of stability studies of steep rock slopes in Europe. Trans. Soc. Min. Engrs. 1973.
7. Bjerrum, I. and Jorstad, R.A. Stability of rock slopes in Norway. Norwegian Geotechnical Institute. Pub. No. 79, Oslo 1968.
8. St.John, C.M. A note on the use of stress distributions in slope stability calculations. Contribution to discussion. Symp. on Open Pit Planning. Johannesburg. 1970.
9. Cundall, P.A. The measurement and analysis of accelerations in rock slopes. Ph.D.Thesis. University of London. 1971.
10. Barton, N.R. A model study of the behaviour of steep excavated rock slopes. Ph.D. Thesis. University of London. 1971.

11. Barton, N.R. Estimation of in situ shear strength from back analysis of failed rock slopes. Symp. of Int. Soc. for Rock Mech. "Fissuration des roches" Nancy, Oct. 1971.
12. Markland, J. Private communication. Rock Mech. Dept., Imp. Coll., London 1970.
13. Mueller, L. The stability of rock bank slopes and the effect of rock water on same. Int. J. Rock Mech. Min. Sci. Vol. I, 1964, pp. 475-504.
14. Ross Brown, D.M. and Barton, N.R. Rock mechanics considerations and the stability of the opencast mines at Rio Tinto, Spain. Imp. Coll. Rock Mech. Res. Rept. No. D7. Sept. 1969, pp. 1-81.
15. Kennedy, B.A. and Niemeyer, K.E. Slope monitoring systems used in the prediction of a major slope failure at the Chuquicamata Mine, Chile. Symp. on Open Pit Planning. Johannesburg 1970.
16. Jennings, J.E. and Robertson, A. Macd. The stability of slopes cut into natural rock. VIIth Int. Conf. Soil Mech. Found. Eng. Mexico 1969, pp. 585-590.
17. Jennings, J.B. A mathematical theory for the calculation of the stability of slopes in open cast mines. Symp. on Open Pit Planning. Johannesburg 1970.
18. Terzaghi, K. Stability of steep slopes on hard unweathered rock. Géotechnique. Vol. XII. No. 4. 1962. pp. 251-270.
19. Hoek, E. Estimating the stability of excavated slopes in opencast mines. Inst. Min. and Metall. Trans. Vol. 79, Oct. 1970, pp. 1094-132A.
20. Barton, N.R. A relationship between joint roughness and joint shear strength. Symp. of Int. Soc. for Rock Mech. "Fissuration des roches", Nancy, Oct. 1971.